Analyst

PAPER

View Article Online
View Journal | View Issue

Cite this: *Analyst*, 2019, **144**, 3552

Direct monitoring of light mediated hyperthermia induced within mammalian tissues using surface enhanced spatially offset Raman spectroscopy (T-SESORS)†

Benjamin Gardner, [a] Pavel Matousek *[b] and Nick Stone *[a]

Received 19th December 2018,
Accepted 16th March 2019

DOI: 10.1039/c8an02466a

rsc.li/analyst

Here we demonstrate light mediated heating of nanoparticles confined deep inside mammalian tissue, whilst directly monitoring their temperature non-invasively using a form of deep Raman spectroscopy, T-SESORS. One of the main barriers to the introduction of photo-thermal therapies (PTT) has been recognised as the inability to directly monitor the local temperature deep within the tissue at the point of therapy. Here Au nanoparticles with a Raman reporter molecule (temperature reporters) are used in combination with Au nanoshells (heat mediators) to provide simultaneously heating under NIR illumination and direct spectroscopic monitoring of local temperature deep within mammalian tissues. The surface enhanced Raman signal was read out at the tissue surface using a transmission geometry in this example and the temperature of the tissue was ascertained from the anti-Stokes to Stokes Raman reporter. This approach opens the prospect of non-invasive hyperthermia treatments with direct temperature feedback from deep inside within tissue, where nanoparticles can be used to both provide localised heating and accurately monitor the local temperature.

Introduction

The field of nanomaterials for photonics applications is rapidly expanding, with increasingly sophisticated materials being developed to monitor a plethora of physical and chemical properties, including but not limited to temperature,[1,2] pH,[3,4] redox,[3] glucose,[5] DNA[6] and proteins such as neurotransmitters,[7] with many of these being complex *in vivo* targets. One such active area is the development of advanced nanomaterials as therapeutics for the next generation of photothermal therapies for cancer treatment.[8,9] The clinical need for such technology stems from the limitations with current photodynamic therapies (PDT), which are largely non-specific for cancer cells, depth limited and/or have various side effects including systemic light sensitivity.[9–11] It is envisioned that nanomaterials would be selectively functionalised to not only specifically target cancer/tumours, utilising appropriate antibodies,[12–17] but also to act simultaneously as a therapeutic agent. This is often considered in the form of photothermal or magnetothermal heating. Furthermore, in the case explored here, a third critical characteristic is considered, where also the temperatures of the nanomaterial can be remotely monitored and controlled non-invasively, even utilising the same energy source as the heating. Potential nanomaterial mediated hyperthermia treatments require the temperature not only to be elevated, but also accurately monitored and maintained within relatively narrow therapeutic thermal windows (41–48 °C) for effective and selective treatments.[9] However, until very recently non-invasive temperature sensing of tissue at depth was not possible[1,2,8,18] representing one of the main barriers to the introduction of photo thermal therapies (PTT).[9] Classically, Raman spectroscopy is seen as a technique limited to the sample surface in diffusely scattering samples such as biological tissues, with the sampling depth often limited to a few hundreds of micrometres. However, with the development of spatially offset Raman spectroscopy (SORS),[19] the closely related inverse SORS,[20,21] as well as resurgence of its variant, transmission Raman (TRS),[22–25] this is no longer the case. These technical developments have radically improved the sampling depth by orders of magnitude demonstrating ability to access depths of several centimetres. The underpinning concept of these techniques constitutes the separation of the illumination and Raman collection zone on the surface of a scattering sample. This allows the contrast of the measured subsurface signal in terms of the surface signal to increase. This has led to a rapid expansion of the field with a variety of

[a]*Biomedical Physics, School of Physics and Astronomy, College of Engineering, Mathematics and Physical Sciences, University of Exeter, Exeter, EX4 4QL, UK. E-mail: n.stone@ex.ac.uk*
[b]*Central Laser Facility, Research Complex at Harwell, STFC Rutherford Appleton Laboratory, Harwell Oxford, OX11 0QX, UK*

†Electronic supplementary information (ESI) available. See DOI: 10.1039/c8an02466a

applications, including non-invasive chemically specific measurements of subsurface temperatures (T-SORS).[18] It is increasingly common to couple SORS/TRS with surface enhanced Raman spectroscopy (SERS),[1,26] in a so called SESORS modality, as this provides a great enhancement of the Raman signal, which is typically weak and further exacerbated when recovering a signal from depth. Recently, we demonstrated the coupling of T-SORS and SERS (T-SESORS) to deliver subsurface temperature probing capability.[1,18] Here we demonstrate the simultaneous heating and non-invasive temperature monitoring of subsurface nanoparticles. The measurement was performed on a combination of two nanoparticle types, co-localised at a depth of 5 mm in porcine tissue 10 mm thick. The bulk temperature of tissue was changed sufficiently (by up to around 20 °C by the addition of the nanoshells) and monitored using the inelastically scattered light to render the approach viable for the potential PTT of the future.

Results and discussion

The Raman spectrum of the Au 100 nm nanoparticles labelled with MBA (the temperature probe) when deposited on CaF_2 is shown in Fig. 1A. This illustrates the spectral range observed and the ν12 benzene ring mode (1085 cm^{-1}) highlighted in red which was used for univariate temperature monitoring purposes throughout. This was selected due to it being the most intense Raman band, minimally overlapping with other Raman bands, *i.e.* porcine tissue signal, and being generally considered invariant to temperature.[27] Initially, the temperature probe was tested alone. As is to be expected (Fig. 1B), when labelled nanoparticles are illuminated with a laser excitation wavelength (830 nm) which is significantly separated from their maximal absorption wavelength (~560 nm), minimal heating is observed (<5 °C). Upon increasing the illumination power, the signal to noise of the measured Raman spectra improved, thus decreasing the spread of the data *i.e.* range of the AS/S ratios measured. Overall, with increasing the power up to 400 mW, there is a minimal change in the nanoparticle temperature.

When the Au-MBA nanoparticles, with a maximal absorption at ~560 nm are co-localised with gold nanoshells (Au-NS), with a maximal absorption at ~800 nm, and illuminated with a 830 nm laser, a clear relationship between illumination power of the laser and the AS/S ratio of the ν12 benzene ring mode of MBA is observed (Fig. 2A & B); for raw Raman spectra see ESI Fig. 1.† At lower power (~250 mW), a very small increase is observed in the AS/S ratio compared to the room temperature baseline established in the absence of the Au-NS (Fig. 1B), indicating a relatively small change in temperature ($\Delta T \sim 5$ °C). However, as the laser power is increased further (500 and 750 mW) a rapid increase in AS/S ratio is evident, before reaching a plateau. The maximal change in temperature corresponds to a ΔT of around 10 °C and 20 °C respectively, as measured by the thermal imaging camera. This indicates that for a thin layer of nanoshells (Au-NS), co-localised with the temperature probe reporter nanoparticles (Au-MBA) on CaF_2, a significant increase in the bulk temperature is seen in the vicinity of the nanoparticles even though only a small proportion of the excitation beam is absorbed as it passes through the sample.

As can be seen (Fig. 3), when Au-MBA labelled nanoparticles alone are inserted in porcine tissue of overall thickness of 10 mm at depth (5 mm), there is a notable increase in temperature observed through changes in the anti-Stokes/Stokes ratio. This increase in temperature is attributed to general photothermal interaction of the laser with tissue constituents *e.g.* water absorption of the illumination beam,[28,29] and not significantly due to the nanoparticles, as previously it was shown there was minimal increase in temperature of the nanoparticles alone with the same power (Fig. 1B). Measuring the anti-Stokes/Stokes ratio and calculating a correction factor, which includes both the effect of instrument response and differential photon absorption in the tissue, at the initial room temperature of 25 °C (see Fig. S1†), the Au-MBA labelled NPs in tissue reach around 40 °C. However, when the heat boosting Au-NS are introduced there is an observable, considerably larger increase in the bulk temperature, measured by the temperature reporters, to approximately 66 °C. This change in the anti-Stokes/Stokes ratios through calibration at the initial equilibrium point is equivalent to a $\Delta T \sim 2$ °C in bulk tissue

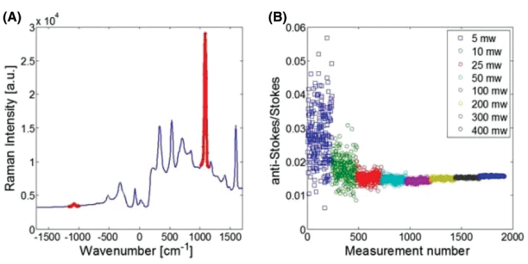

Fig. 1 (A) Raman spectrum of Au-MBA nanoparticles alone deposited on CaF_2 with the (1085 cm^{-1} ν12 benzene ring mode) highlighted in red. (B) anti-Stokes/Stokes intensity ratio (ν12 benzene ring mode) of MBA labelled gold nanoparticles alone deposited on CaF_2 measured between 5–400 mW at 830 nm excitation.

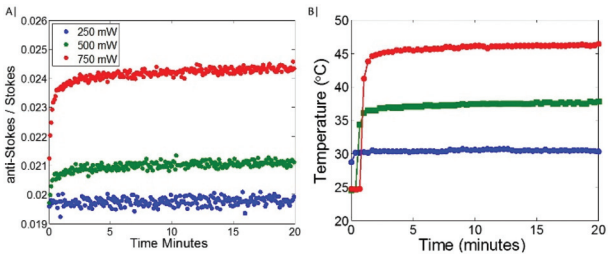

Fig. 2 (A) Anti-Stokes/Stokes intensity ratio of the 1085 cm^{-1} ν12 benzene ring mode of Au-MBA labelled nanoparticles co-localised with NIR absorbing Au-NS deposited on CaF_2, under different illumination powers (250, 500 and 750 mW) at 830 λ_{ex}. (B) Peak temperature of the Au-MBA and Au-NS while illuminated with 830 λ_{ex} beam under different laser powers (blue 250 mW, green 500 mW and red 750 mW) measured by thermal imaging camera.

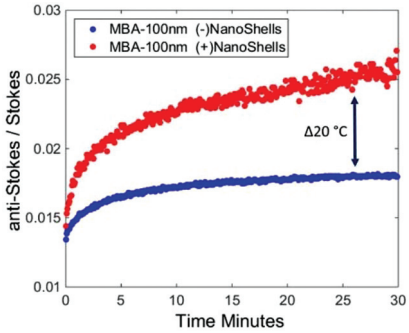

Fig. 3 Anti-Stokes/Stokes ratio of (1085 cm^{-1} ν12 benzene ring mode) temperature reporter Au-MBA nanoparticles in the absence (blue) and presence (red) of Au-NS with a peak absorbance at 800 nm while inserted in porcine tissue at a depth of 5 mm (with a total thickness of 10 mm) and illuminated with 1.2 W (λ_{ex} 830 nm). See ESI Fig. 2A & B† for corresponding raw Raman data.

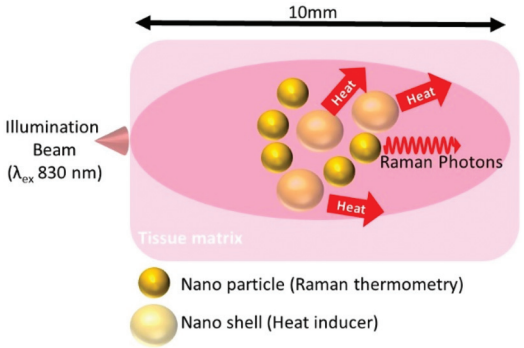

Fig. 4 Schematic of non-invasive Raman thermometry at depth in porcine tissue using labelled nanoparticles (Au-MBA) monitoring temperature changes induced by gold nanoshells (Au-NS).

temperature caused by the nanoshells as opposed to non-specific heating. This temperature increase is well within the range required to elevate natural temperature tissue *in vivo* to the required therapeutic window range (which is ideally 41–48 °C), demonstrating that either lower powers or treatment of deeper lesions is clearly viable.

Experimental

Temperature reporters were made up of 100 nm diameter gold citrate coated nanoparticles (0.05 mg ml^{-1}) (NanoComposix) λ_{max} 563 nm, labelled with mercaptobenzoic acid (Sigma Aldrich) (Au-MBA) using a previously described method.[30] In brief 100 µl of 1 mM MBA in EtoH was added to 1 ml of the nanoparticle suspension, the sample was mixed for 5 min before centrifugation at 3000 rpm for 10 min. For demonstration of photothermal heating, the Au-MBA nanoparticles were combined with 4 ml of (0.05 mg ml^{-1}) polyvinylpyrrolidone (PVP) coated gold nanoshells (Au-NS) λ_{max} 800 nm. Raman measurements were carried out on a homebuilt instrument, operating in transmission Raman geometry. In brief, a tuneable Ti:Sapphire laser (Newport, Spectra Physics) generated a laser beam at 830 nm. The beam was passed through a NIR acousto-optic tuneable filter (Gooch and Housego) to clean up spectrally the laser line. Following transmission through the sample the laser line was suppressed with two 830 nm notch filters (Kaiser) and the signal was collected using a deep depletion CCD camera (Andor iDus-420) which was coupled to a high throughput Raman spectrometer (Kaiser Holospec 1.8i) operating with a custom low dispersive holographic transmission grating (Kaiser). Raman spectra were collected for 5 s (10 accumulations of 0.5 s). Initial measurements testing the heating of the non-NIR absorbing temperature reporter NPs (Au-MBA) was undertaken by depositing them onto a CaF_2 slide and measuring the anti-Stokes/Stokes (AS/S) ratio and the surface temperature with an infrared temperature sensor (PyroMiniusb), as well as a thermal imaging camera (T430, FLIR). The illumination power at 830 nm was varied between 5 to 400 mW to explore the measured AS/S ratio *versus* power and its relationship with temperature. To monitor temperature induced by the NIR absorbing nano shells, the Au-MBA temperature reporter and the nanoshells were mixed together and deposited onto CaF_2 and left to dry. The mixture was monitored at three separate powers 250, 500 & 750 mW. The AS/S ratio of the reporter was monitored simultaneously with temperature monitors (infrared sensor, thermal imaging camera). To monitor temperature noninvasively at depth, the temperature reporter (Au-MBA) was deposited in the middle of 10 mm thick porcine tissue with and without nanoshells present (Fig. 4).

The depth experiments were carried out with 1.2 W illumination power at the tissue surface (a laser beam diameter of 1 mm) and the at depth temperature being monitored noninvasively throughout by the aforementioned temperature monitors. As has been reported in previous work[1,18] a calibration point is required for temperature measurements at depth using Raman, which in this example was taken from time point one (at the onset of illumination), a reflection of the closest equilibrium temperature point, *i.e.* ambient temperature or body temperature for *in vivo* applications. This is due to the significant difference in wavelength of the anti-Stokes & Stokes photons ~150 nm in this case, the photons experience significant differences in absorption and scattering over the large photon pathlengths in scattering media (tissue) as well as being affected differently by the instrument response function; both effects changing the expected theoretical ratiometric information.[25] The use of simple scaling factors derived from this first equilibrium temperature measurement eloquently solves this otherwise complex issue of calibrating the anti-Stokes/Stokes ratio to temperature (see ESI Fig. 3†). This is analogous to requiring emissivity information for thermal IR cameras to accurately report temperature.

Conclusions

This proof of concept demonstrates how deep Raman can not only be used to non-invasively monitor temperature at depth,

with chemical specificity if needed, but also be used as a tool to control the photothermal dose to the treatment zone. This can be achieved in real-time, to ensure optimum benefit is achieved and minimum damage to surrounding tissues. This is of increasing relevance for advancements in disease treatments such as cancer as, to date, one of the main barriers to the introduction of PTT has been recognised to be the inability to directly monitor the local temperature within the tissue.

Conflicts of interest

There are no conflicts to declare.

Acknowledgements

EPSRC grants (EP/K020374/1 and EP/P012442/1) partly funded the work presented here. The research data supporting this publication are provided within this paper.

Notes and references

1 B. Gardner, N. Stone and P. Matousek, *Faraday Discuss.*, 2016, **187**, 329–339.
2 E. A. Pozzi, A. B. Zrimsek, C. M. Lethiec, G. C. Schatz, M. C. Hersam and R. P. Van Duyne, *J. Phys. Chem. C*, 2015, **119**, 21116–21124.
3 L. E. Jamieson, V. L. Camus, P. O. Bagnaninchi, K. M. Fisher, G. D. Stewart, W. H. Nailon, D. B. McLaren, D. J. Harrison and C. J. Campbell, *Nanoscale*, 2016, **8**, 16710–16718.
4 X. S. Zheng, P. Hu, Y. Cui, C. Zong, J. M. Feng, X. Wang and B. Ren, *Anal. Chem.*, 2014, **86**, 12250–12257.
5 C. R. Yonzon, C. L. Haynes, X. Zhang, J. T. Walsh and R. P. Van Duyne, *Anal. Chem.*, 2004, **76**, 78–85.
6 S. Tian, O. Neumann, M. J. McClain, X. Yang, L. Zhou, C. Zhang, P. Nordlander and N. J. Halas, *Nano Lett.*, 2017, **17**, 5071–5077.
7 A. S. Moody, P. C. Baghernejad, K. R. Webb and B. Sharma, *Anal. Chem.*, 2017, **89**, 5688–5692.
8 J. Kneipp, *ACS Nano*, 2017, **11**, 1136–1141.
9 D. Jaque, L. Martínez Maestro, B. del Rosal, P. Haro-Gonzalez, A. Benayas, J. L. Plaza, E. Martín Rodríguez, J. García Solé, L. Martinez Maestro, B. del Rosal, P. Haro-Gonzalez, A. Benayas, J. L. Plaza, E. Martin Rodriguez and J. Garcia Sole, *Nanoscale*, 2014, **6**, 9494–9530.
10 J. Dobson, G. F. de Queiroz and J. P. Golding, *Vet. J.*, 2018, **233**, 8–18.
11 M. B. Vrouenraets, G. W. Visser, G. B. Snow and G. A. van Dongen, *Basic principles, applications in oncology and improved selectivity of photodynamic therapy*, 2003, vol. 23.
12 S. Pahlow, K. Weber, J. Popp, B. R. Wood, K. Kochan, A. Rüther, D. Perez-Guaita, P. Heraud, N. Stone, A. Dudgeon, B. Gardner, R. Reddy, D. Mayerich and R. Bhargava, *Appl. Spectrosc.*, 2018, **72**(1_suppl), 52–84.
13 K. J. Yoon, H. K. Seo, H. Hwang, D. Pyo, I.-Y. Eom, J. H. Hahn and Y. M. Jung, *Bull. Korean Chem. Soc.*, 2010, **31**, 1215–1218.
14 S. Chen, C. Bao, C. Zhang, Y. Yang, K. Wang, B. V. Chikkaveeraiah, Z. Wang, X. Huang, F. Pan, K. Wang, X. Zhi, J. Ni, J. M. de la Fuente and J. Tian, *Nano Biomed. Eng.*, 2016, **8**, 315–328.
15 A. Samanta, K. K. Maiti, K.-S. Soh, X. Liao, M. Vendrell, U. S. Dinish, S.-W. Yun, R. Bhuvaneswari, H. Kim, S. Rautela, J. Chung, M. Olivo and Y.-T. Chang, *Angew. Chem., Int. Ed.*, 2011, **50**, 6089–6092.
16 Z. Chen, M.-F. Penet, S. Nimmagadda, C. Li, S. R. Banerjee, P. T. Winnard, D. Artemov, K. Glunde, M. G. Pomper and Z. M. Bhujwalla, *ACS Nano*, 2012, **6**, 7752–7762.
17 A. Oseledchyk, C. Andreou, M. A. Wall and M. F. Kircher, *ACS Nano*, 2017, **11**, 1488–1497.
18 B. Gardner, P. Matousek and N. Stone, *Anal. Chem.*, 2016, **88**, 832–837.
19 P. Matousek, I. P. Clark, E. R. C. Draper, M. D. Morris, A. E. Goodship, N. Everall, M. Towrie, W. F. Finney and A. W. Parker, *Appl. Spectrosc.*, 2005, **59**, 393–400.
20 P. Matousek and N. Stone, *J. Biophotonics*, 2013, **6**, 7–19.
21 M. V. Schulmerich, K. A. Dooley, M. D. Morris, T. M. Vanasse and S. A. Goldstein, *J. Biomed. Opt.*, 2006, **11**, 060502.
22 M. M. Kerssens, P. Matousek, K. Rogers and N. Stone, *Analyst*, 2010, **135**, 3156.
23 M. Z. Vardaki, H. Sheridan, N. Stone and P. Matousek, *Appl. Spectrosc.*, 2017, **71**, 1849–1855.
24 N. Stone and P. Matousek, *Cancer Res.*, 2008, **68**, 4424–4430.
25 B. Gardner, N. Stone and P. Matousek, *Anal. Chem.*, 2017, **89**, 9730–9733.
26 H. N. Xie, R. Stevenson, N. Stone, A. Hernandez-Santana, K. Faulds and D. Graham, *Angew. Chem., Int. Ed.*, 2012, **51**, 8509–8511.
27 A. Williams, K. J. Flynn, Z. Xia and P. R. Dunstan, *J. Raman Spectrosc.*, 2016, **47**, 819–827.
28 R. A. Chipman, *OSA Handb., Opt. - Vol II*, 1995, pp. 22.1–22.35.
29 M. Nourhashemi, M. Mahmoudzadeh and F. Wallois, *Neurophotonics*, 2016, **3**, 015001.
30 A. Jaworska, L. E. Jamieson, K. Malek, C. J. Campbell, J. Choo, S. Chlopicki and M. Baranska, *Analyst*, 2014, **140**, 2321–2329.